Sparsity-Driven Frequency Diverse MIMO Radar Imaging for Moving Targets

Xuezhi He, Bo Liu, and Dongjin Wang

Abstract—By synthesizing multiple frequency signals into a wideband signal, the frequency diverse multiple-input-multiple-output (FD-MIMO) radar can obtain higher resolution than ordinary MIMO radar. Furthermore, FD-MIMO radar can obtain higher resolution and better recovery performance by exploiting the sparsity of the targets. For moving targets with unknown velocities, the recovery performance based on compressive sensing (CS) would significantly degrade if the estimation accuracy of velocities is not enough. We propose a new approach of adaptive sparse recovery via velocity estimation (ASR-VE) for multiple moving targets FD-MIMO radar imaging. ASR-VE estimates the scattering coefficients as well as the unknown velocities involved in the sensing matrix in the loop iterations. Numerical simulations are carried out to verify the effectiveness of the proposed method.

***Index Terms*—MIMO radar imaging, moving targets, sparse recovery, velocity estimation.**

I. Introduction

Multiple-input-multiple-output (MIMO) radar system has attracted much attention recently due to the additional degrees of freedom and the higher spatial resolution [1]. Moreover, MIMO radar system with frequency diversity (FD-MIMO) has been researched widely [2], [3], since its range resolution can be further improved by simultaneously fusing the echoes coming from different transmitters to form a wideband signal.

In most radar imaging applications, the scatterers of the target are often sparsely distributed. Using compressive sensing (CS) based sparse recovery techniques, higher resolution and better recovery performance can be obtained by exploiting the sparsity of the scatterers [4], [5]. Generally, CS casts the sparse recovery problem as an estimation problem corresponding to $y=\Phi x+e$, where $\boldsymbol{y}$ is the echoes received, $\boldsymbol{e}$ is the additive noise, Φ is the sensing matrix, and $\boldsymbol{x}$ is the unknowns to be recovered. CS searches for the sparsest $\boldsymbol{x}$, i.e. the solution with least non-zero entries.

MIMO radar imaging for moving targets has been developed in [6], [7]. Since the sensing matrix Φ is effected by the velocities, if the velocities are not accurately estimated, Φ can mismatch the actual one and then degrade the sparse recovery performance. Chi *et al.* [8] verify that the sparse recovery performance is likely to suffer from a large error when the mismatch of the sensing matrix exists. Hence, it is crucial to estimate the velocities and eliminate the mismatch in the sensing matrix. [9], [10] use an overcomplete dictionary approach to jointly estimate the scattering coefficients and velocities by constructing a grid of possible scatter velocities at each location. However, the estimation problem would be time-consuming due to the enlargement of the unknowns vector, and also the estimation accuracy would be determined by the discretization level of the velocities. If the case of the off-grid velocity exists, the sparse recovery performance would be deteriorated [11].

In this paper we derive the model of FD-MIMO radar imaging for multiple moving targets and develop an improved iterative alternating approach of adaptive sparse recovery via velocity estimation (ASR-VE). ASR-VE estimates the scattering coefficients as well as the unknown velocities involved in the sensing matrix in the loop iterations. Simulation results verify the effectiveness of the proposed method.

Notation: $(\bullet)^H$, *vec*$(\bullet)$ denote the conjugate transpose, and the vectorization operation, respectively. $\| x \|_p$ denote the l_p norm of a vector x. $\| A \|_2$ is the spectral norm of the matrix A. diag($\boldsymbol{x}$) is a diagonal matrix with its diagonal entries being entries of a vector x.

II. Problem Formulation

The scenario of MIMO radar system composed by M transmitters and N receivers is illustrated in Fig. 1. For simplicity, uniform linear arrays (ULA) are considered with inter-element spacing given by d_t=Nd and d_r=d, respectively. Here we focus our derivation on the linear frequency modulated (LFM) based FD-MIMO radar imaging. The different transmitter elements transmit LFM signals within different bands respectively.

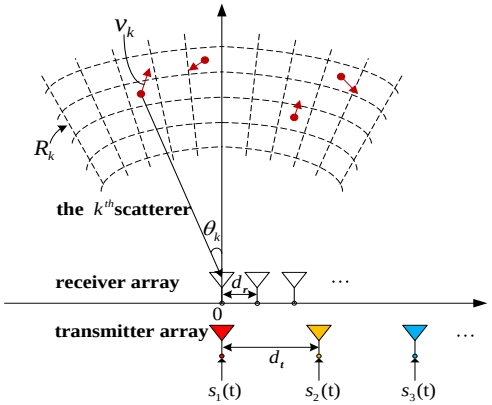

Fig. 1. Imaging scenario for moving targets FD-MIMO radar

Define $s(t)=[s_1(t), s_2(t),\ldots, s_M(t)]^T$ where $s_m(t)$ indicates the LFM waveform for the m^{th} transmitter,

Manuscript received November 8, 2012; revised December 24, 2012. This

He Xuezhi, Liu Bo, and Wang Dongjin are with Department of Electronic Engineering and Information Science, University of Science and Technology of China, Hefei, Anhui, P. R. China (e-mail: hexz@mail.ustc.edu.cn).

DOI: 10.7763/IJIEE.2013.V3.346

$$s_m(t)=rect\left(t/T_s\right)\exp\left[\mathrm{j}2\pi\left(f_m t+0.5\gamma t^2\right)\right] \quad (1)$$

where γ is the chirp rate, f_m is the carrier frequency of the m-th transmitter, $f_m = f_c+m\gamma T_s$. f_c, T_s represent the reference carrier frequency and the pulse duration, respectively. Rect (•) is the rectangular window with the pulse duration T_s.

We assume the targets are located in the far-field and the imaging scene contains U radial range bins and V angle bins. Setting $K=UV$, and supposing that the targets are moving at time-invariant velocities, we define σ_κ, $R_{\kappa,0}$, $\theta_{\kappa,0}$, v_k (for κ=1,2,...,K) as the scattering coefficient, the initial radial range, the initial impinging angle and the velocity, respectively. The targets are sparsely distributed, apparently, if no scatterer is at the k^{th} grid bin, then $\sigma_\kappa=0$, $v_k=0$.

The echoes of N receivers $z(t)= [z_1(t), z_2(t),\ldots, z_N(t)]^T$ can be written in the following form,

$$\boldsymbol{z}(t)=\sum_{k=1}^{K}\sigma_k\boldsymbol{b}(\theta_k(t))\boldsymbol{a}^T(\theta_k(t))\boldsymbol{s}\left(t-\frac{2R_k(t)}{c}\right)+\boldsymbol{e}(t) \quad (2)$$

where e(t) is the additive noise. The terms $\{\boldsymbol{a}(\theta_\kappa)\}$ and $\{\boldsymbol{b}(\theta_\kappa)\}$ refer to the transmit and receive steering vectors, respectively. Assuming that the bandwidth of each LFM signal $B=\gamma T_s$ is narrow and the imaging scene is small, then $\{\boldsymbol{a}(\theta_\kappa)\}$ and $\{\boldsymbol{b}(\theta_\kappa)\}$ can be described by (3),

$$\begin{aligned}\boldsymbol{a}(\theta_k)&=\left[1,\exp\left(-j\frac{2\pi f_c d_t\theta_k}{c}\right),\cdots,\exp\left(-j\frac{2\pi f_c d_{tM}\theta_k}{c}\right)\right]^T\\ \boldsymbol{b}(\theta_k)&=\left[1,\exp\left(-j\frac{2\pi f_c d_r\theta_k}{c}\right),\cdots,\exp\left(-j\frac{2\pi f_c d_{rN}\theta_k}{c}\right)\right]^T\end{aligned} \quad (3)$$

where $d_{tM}=(M-1)d_t$, $d_{rN}=(N-1)d_r$.

After orthogonal separation, we can obtain the echo signal corresponding to the m^{th} transmitter and the n^{th} receiver as

$$z_{mn}(t)=\sum_{k=1}^{K}\sigma_k b_n(\theta_k(t))a_m(\theta_k(t))s_m\left(t-\frac{2R_k(t)}{c}\right)+e_{mn}(t) \quad (4)$$

where $a_m(\theta_\kappa)$ is the m-th element of $\{a(\theta_\kappa)\}$, $b_n(\theta_\kappa)$ is the n-th element of $\{b(\theta_\kappa)\}$.

We are also assuming that the velocities of the targets are small enough so that their displacement during a pulse period can be neglected. This assumption is well justified, and has been shown not to affect the estimation performance [12]. Supposing that the reference range is R_0, for LFM signal, we have

$$\begin{aligned}&s_m\left(t-\frac{2R_k(t)}{c}\right)s_m^*\left(t-\frac{2R_0}{c}\right)\\ &\approx \mathrm{rect}\left(\frac{t'}{T}\right)\exp\left\{-j\frac{4\pi}{c}\left[(f_m+\gamma t')r_k(t)-\frac{\gamma}{c}r_k^2(t)\right]\right\}\end{aligned} \quad (5)$$

where $t'=t-2R_0/c$, $r_\kappa(t)=R_\kappa(t)-R_0$. Define $v_k=[v_{R,k}, v_{\theta,k}]<<c$, where c is the speed of light, then the instantaneous position of the k^{th} scatterer can be written as $R_\kappa(t)=R_{\kappa,0}+v_{R,k}t$, $\theta_\kappa(t)=\theta_{\kappa,0}+v_{\theta,k}t/R_0$. After dechirping and removing the residual video phase in (5) according to [13], for the q^{th} (q=0,2,...,Q-1) snapshot (the sampling interval is T_r, which is the same as the pulse repetition period), we have

$$z_{mnq}=\sum_{k=1}^{K}\sigma_k\exp\left\{-j2\pi\left[\begin{array}{l}\frac{2(f_m+\gamma qT_s)}{c}\left(r_{k,0}+v_{R,k}qT_r\right)+\\ \frac{f_c(d_{tm}+d_{rn})}{c}\left(\theta_{k,0}+v_{\theta,k}qT_r/R_0\right)\end{array}\right]\right\}+e_{mnq} \quad (6)$$

where we set $t_0=2R_0/c$ as the initial moment. The elements of the echoes are index by the tuple (m, n, q), with q being the sampling times associated with the mn^{th} transmit-receive pair.

Define $z=vec(z_{\text{mnq}})$ with its size MNQ×1, $e=vec(e_{\text{mnq}})$ with the same size, then set

$$\boldsymbol{\Phi}_k=vec\left(\exp\left\{-j2\pi\left[\begin{array}{l}\frac{2(f_m+\gamma qT_s)}{c}\left(r_{k,0}+v_{R,k}qT_r\right)+\\ \frac{f_c(d_{tm}+d_{rn})}{c}\left(\theta_{k,0}+v_{\theta,k}qT_r/R_0\right)\end{array}\right]\right\}\right) \quad (7)$$

Moreover, we let $\Phi=(\Phi_1,\Phi_2,\ldots,\Phi_K)$, we can know that the sensing matrix Φ is determined by the transceiver configuration, the transmitting signal and the unknown velocities, so we describe $\Phi=\Phi(v)$, where $v=[v_R, v_\theta]^T$, $v_R=[v_{R,1}, v_{R,2},..., v_{R,K}]$, $v_\theta=[v_{\theta,1}, v_{\theta,2},..., v_{\theta,K}]$.

Then the echoes can be redefined as

$$\boldsymbol{z}=\boldsymbol{\Phi}(\boldsymbol{v})\boldsymbol{\sigma}+\boldsymbol{e} \quad (8)$$

While the scattering coefficients $\boldsymbol{\sigma}$ enter the problem linearly, the unknown velocities $\boldsymbol{v}$ do not, so the overall problem is nonlinear and coupled. When the velocity is ignored (set to zero) or set to an incorrect value, the target recovery exhibits defocusing of the energy of the moving scatterer [14]. Therefore, we propose a new approach of adaptive sparse recovery via velocity estimation (ASR-VE) to solve the under-determined and non-linear problem.

III. Sparse Recovery Approach

With the constraint that $\boldsymbol{\sigma}$ is a sparse vector, (8) can be well solved by sparse recovery techniques. Compared to $\|\boldsymbol{\sigma}\|_1$, using $\|\boldsymbol{\sigma}\|_p$(0<p<1) can get sparser solution, so we use $\|\boldsymbol{\sigma}\|_p$(0<p<1) for sparse punishment, then the corresponding optimization problem is written as

$$\hat{\boldsymbol{\sigma}},\hat{\boldsymbol{v}}=\arg\min\left\|\boldsymbol{\sigma}\right\|_p^p, s.t.\left\|\boldsymbol{z}-\boldsymbol{\Phi}(\boldsymbol{v})\boldsymbol{\sigma}\right\|_2^2\le\varepsilon \quad (9)$$

where ε is the noise power. Since (9) is a non-linear problem, in the ASR-VE framework we use an iterative loop to solve it. Detailed algorithm is stated as follows.

A. Step 1: Sparse Recovery

Assuming that $\boldsymbol{v}^{(l)}$ are obtained, where l is the counter of iteration, we seek for the optimal $\sigma^{(l+1)}$ to minimize the following equivalent cost function,

$$F_1\left(\boldsymbol{\sigma}^{(l+1)}\right)=\left\|\boldsymbol{\sigma}^{(l+1)}\right\|_p^p+\frac{1}{\varepsilon}\left\|\boldsymbol{z}-\boldsymbol{\Phi}\left(\boldsymbol{v}^{(l)}\right)\boldsymbol{\sigma}^{(l+1)}\right\|_2^2 \quad (10)$$

Letting $dF_1/d\sigma^{(l+1)}=0$, defining $\alpha=p\zeta^{(l)}/2$, from (10), we can get that [15]

$$\boldsymbol{\sigma}^{(l+1)}=\boldsymbol{W}\left(\left(\boldsymbol{\Phi W}\right)^H\boldsymbol{\Phi W}+\alpha\boldsymbol{I}\right)^{-1}\left(\boldsymbol{\Phi W}\right)^H\boldsymbol{z} \quad (11)$$

where *we indicate* $W=W(\sigma^{(l+1)})$, $\Phi=\Phi(v^{(l)})$ for simplicity, and

$$\boldsymbol{W}=\boldsymbol{W}\left(\boldsymbol{\sigma}^{(l+1)}\right)=diag\left\{\left|\sigma_1^{(l+1)}\right|^{1-p/2},\left|\sigma_2^{(l+1)}\right|^{1-p/2},...,\left|\sigma_K^{(l+1)}\right|^{1-p/2}\right\} \quad (12)$$

Using iterative relaxation method, we can get the recursion formula corresponding to $\sigma^{(l+1)}$,

$$\boldsymbol{\sigma}^{(l+1,s)}=\boldsymbol{W}^{(l,s)}\left(\left(\boldsymbol{\Phi W}^{(l,s)}\right)^H\boldsymbol{\Phi W}^{(l,s)}+\alpha\boldsymbol{I}\right)^{-1}\left(\boldsymbol{\Phi W}^{(l,s)}\right)^H\boldsymbol{z} \quad (13)$$

where s is the internal iteration index, and $\boldsymbol{W}^{(l,s=0)}=\boldsymbol{W}(\boldsymbol{\sigma}^{(l)})$.

Moreover, considering $MNQ<K$, with the aid of matrix inversion formula [16], we can get the recursion formula corresponding to $\boldsymbol{\sigma}^{(l+1)}$,

$$\boldsymbol{\sigma}^{(l+1,s)}=\left(\boldsymbol{W}^{(l,s)}\right)^2\left(\boldsymbol{\Phi}\left(\boldsymbol{v}^{(l)}\right)\right)^H\left(\boldsymbol{\Phi}\left(\boldsymbol{v}^{(l)}\right)\left(\boldsymbol{W}^{(l,s)}\right)^2\left(\boldsymbol{\Phi}\left(\boldsymbol{v}^{(l)}\right)\right)^H+\alpha\boldsymbol{I}\right)^{-1}\boldsymbol{z} \quad (14)$$

The internal iteration about s stops when $\boldsymbol{\sigma}^{(l+1,s)}$ converges, yielding $\boldsymbol{\sigma}^{(l+1)}$.

B. Step 2: Velocity Estimation

After getting $\boldsymbol{v}^{(l)}$, $\boldsymbol{\sigma}^{(l+1)}$, we linearize $\boldsymbol{\Phi}(v)$ at local neighborhood of $\boldsymbol{v}^{(l)}$ with Taylor expansion,

$$\boldsymbol{\Phi}\left(\boldsymbol{v}\right)=\boldsymbol{\Phi}\left(\boldsymbol{v}^{(l)}+\Delta\boldsymbol{v}\right)\approx\boldsymbol{\Phi}\left(\boldsymbol{v}^{(l)}\right)+\boldsymbol{\psi}_R^{(l)}\Delta\boldsymbol{v}_R+\boldsymbol{\psi}_\theta^{(l)}\Delta\boldsymbol{v}_\theta \quad (15)$$

where $\boldsymbol{\psi}_R^{(l)}=\partial\boldsymbol{\Phi}\left(\boldsymbol{v}\right)/\partial\boldsymbol{v}_R\big|_{\boldsymbol{v}=\boldsymbol{v}^{(l)}}$, $\boldsymbol{\psi}_\theta^{(l)}=\partial\boldsymbol{\Phi}\left(\boldsymbol{v}\right)/\partial\boldsymbol{v}_\theta\big|_{\boldsymbol{v}=\boldsymbol{v}^{(l)}}$.

Define $\boldsymbol{\psi}^{(l)}=\left[\boldsymbol{\psi}_R^{(l)}\cdot diag\left(\boldsymbol{\sigma}^{(l)}\right),\boldsymbol{\psi}_\theta^{(l)}\cdot diag\left(\boldsymbol{\sigma}^{(l)}\right)\right]^T$, $\Delta\boldsymbol{v}=[\Delta\boldsymbol{v}_R,\Delta\boldsymbol{v}_\theta]^T$, then we search for optimized $\Delta\boldsymbol{v}$ corresponding to

$$\Delta v^{(l+1)}=\arg\min_{\Delta\boldsymbol{v}}\left\|\boldsymbol{z}-\boldsymbol{\Phi}\left(\boldsymbol{v}^{(l)}\right)\boldsymbol{\sigma}^{(l)}+\boldsymbol{\psi}^{(l)}\Delta\boldsymbol{v}\right\|_2^2 \quad (16)$$

From (16), we can get

$$\Delta v^{(l+1)}=\frac{\mathrm{Re}\left[\left(\boldsymbol{\psi}^{(l)}\right)^H\left(\boldsymbol{z}-\boldsymbol{\Phi}\left(\boldsymbol{v}^{(l)}\right)\boldsymbol{\sigma}^{(l)}\right)\right]}{\mathrm{Re}\left[\left(\boldsymbol{\psi}^{(l)}\right)^H\boldsymbol{\psi}^{(l)}\right]} \quad (17)$$

So we can get the velocity estimation results as

$$v^{(l+1)}=v^{(l)}+\Delta v^{(l+1)} \quad (18)$$

C. Step 3: Adaptive Update for Norm p

The recovery performance depends on selection of norm value p. To make norm p sensitive to the convergence, we make an adaptive update for p. Defining Normalized Mean Square Error ($NMSE^{(l)}=\left\|\boldsymbol{\sigma}^{(l+1)}-\boldsymbol{\sigma}^{(l)}\right\|_2^2/\left\|\boldsymbol{\sigma}^{(l)}\right\|_2^2$), we then update p as

$$p^{(l+1)}=p^{(l)}+\beta\frac{NMSE^{(l)}-NMSE^{(l-1)}}{NMSE^{(l)}} \quad (19)$$

where β indicates a positive constant to control the incidence of NMSE.

Then, set $l\rightarrow l+1$ and repeat the three stages above until ASR-VE shows no obvious improvement.

Through alternating iteration, ASR-VE turns the non-linear optimization problem to a linear optimization problem. In the first step of sparse recovery, it is shown in [15] that when $\boldsymbol{\sigma}^{(l)}$ is transformed to $\boldsymbol{\sigma}^{(l+1)}$, the cost function of $\boldsymbol{F}_1$ decreases. The second step of velocity estimation is a least-square problem, so the cost function also decreases. To accelerate the convergence of ASR-VE, we add an adaptive update process for norm p.

The sketch of ASR-VE is as follows:

TABLE I: THE SKETCH OF ASR-VE

Adaptive sparse recovery via velocity estimation (ASR-VE)

Input: $\boldsymbol{z}$, $\Phi^{(0)}=\Phi(v=0)$;

Initialization:

$\boldsymbol{\sigma}_j^{(0)}=\left(\left(\boldsymbol{\Phi}_j^{(0)}\right)^H\boldsymbol{\Phi}_j^{(0)}\right)^{-1}\left(\boldsymbol{\Phi}_j^{(0)}\right)^H\boldsymbol{z}$, (j=1,...,K), $v^{(0)}=0$, $\varepsilon=0.01$;

Iteration (denote l as the counter of iteration):

i. estimate $\sigma^{(l+1)}$ by (14);
ii. calculate $v^{(l+1)}$ by (18);
iii. update $p^{(l+1)}$ by (19);
iv. $l\rightarrow l+1$;
v. end: The loops are terminated when the norm of σ changes moderately between the adjacent loop.

Output: $\sigma=\sigma^{(L+1)}$, $v=v^{(L+1)}$.

IV. SIMULATION RESULTS

In this section, we present several numerical simulation results to illustrate the performance of the proposed algorithm. The simulation conditions are given in Table Ⅱ. From Table Ⅱ, we know that the wavenumber-domain coverage is $(2MB/c, (MN-1)df_c/c)$ [17], so we set the range bin $\rho_r=c/(2MB)=1m$, and the angle bin $\rho_\theta=\boldsymbol{c}/\left((MN-1)df_c\right)\approx 0.001rad$. The signal to noise ratio (SNR) is set to be 20dB.

TABLE Ⅱ: SIMULATION CONDITIONS

Parameter	Value
Number of transmitters M	10
Number of receivers N	10
Bandwidth of each transmitted signal B	15MHz
Pulse duration T_s	5us
Pulse repetition period T_r	5ms
Number of snapshots Q	15
Carrier frequency of the first transmitter f_c	10GHz
inter-element spacing of the transmitters d_t	3m
inter-element spacing of the receivers d_r	0.3m
reference range R_0	1km

The original scatterer distribution of the targets is shown in Fig. 2. There are U=40 radial range bins and V =40 angle bins. And there are 10 scatterers with unit scattering coefficient in

the scene of interest. The velocities is given in Table III.

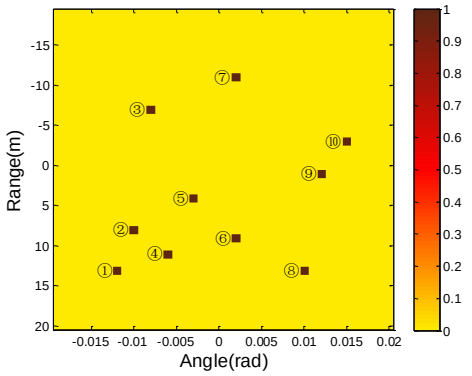

Fig. 2. Scatterer distribution of the targets

TABLE III: THE VELOCITIES OF SCATTERERS

Scatterer	Amplitude of Velocity (m/s)	Range component of velocity (m/s)	Angle component of velocity (rad/s)
①	20	-16	12×10^{-3}
②	20	-16	12×10^{-3}
③	36.8	26	-26×10^{-3}
④	20	-16	12×10^{-3}
⑤	0	0	0
⑥	22.7	16	16×10^{-3}
⑦	32.5	28.1	-16.3×10^{-3}
⑧	0	0	0
⑨	26.4	13.2	22.9×10^{-3}
⑩	26.4	13.2	22.9×10^{-3}

Here, we consider four techniques, namely, the standard matched filtering (MF) approach, orthogonal matching pursuit (OMP), overcomplete dictionary (OCD) reconstruction method [9] and ASR-VE. OCD introduces an appropriate overcomplete dictionary of velocity hypotheses by constructing a grid of possible scatter velocities at each location. Then the unknown vector is extended to contain all possible scatterer velocities and locations.

Firstly, to confirm that it is crucial to make good velocity estimation to get good sparse recovery performance, we present the imaging results of multiple moving targets while the velocities are ignored or known precisely using MF and OMP. The results are shown in Fig. 3. The imaging results by MF totally fail because of the incomplete wavenumber-domain coverage whatever the velocities are ignored or known precisely. The imaging results by OMP show that the reconstructed targets are blurred caused by ignoring the velocity information, however, if the velocity information is known precisely, good imaging performance can be obtained.

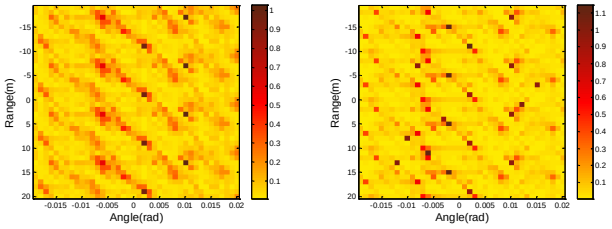

(a) (b)

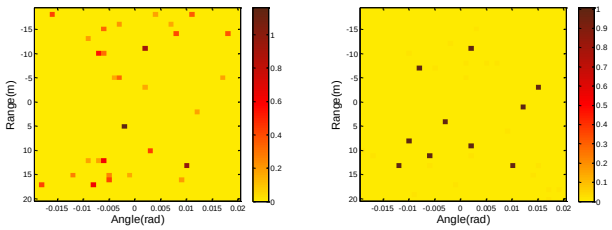

(c) (d)

Fig. 3. (a) Imaging result by MF in the case of ignoring velocities,
(b) Imaging result by MF in the case of known velocities,
(c) Imaging result by OMP in the case of ignoring velocities,
(d) Imaging result by OMP in the case of known velocities.

Secondly, we present the sparse recovery results by the proposed method (ASR-VE) and OCD given in Fig. 4. ASR-VE and OCD methods are likely to obtain good recovery performance since the velocities are estimated. the imaging results of ASR-VE surpass that of OCD because we can get more accurate velocity estimation and sparser solution.

Finally, we calculate the normalized Mean Square Error (NMSE) of target recovery and velocity estimation results versus different SNR. The SNR varies from 0dB to 40dB with interval 5dB. The results shown in Fig. 5 are averaged over 30 independent trials. From Fig. 5, it can be seen that the target recovery errors by MF, OMP always maintain a high level, even when the SNR increases, this is because the velocity information can't be estimated. However, ASR-VE and OCD can get improved target recovery and also velocity estimation results when the SNR is greater than 15dB. ASR-VE also surpasses that of OCD, which illustrates that ASR-VE is more robust to noise.

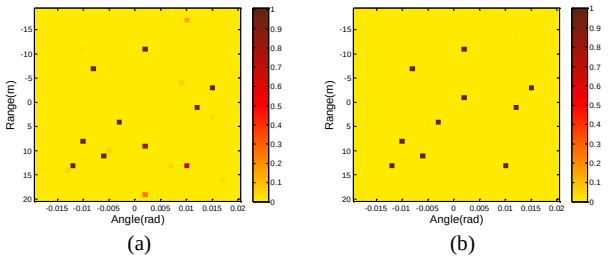

(a) (b)

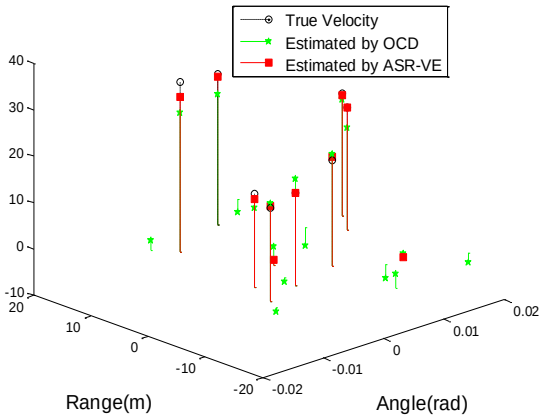

(c)

Fig. 4. (a) Target recovery result by OCD,
(b) Target recovery result by ASR-VE,
(c) Velocity estimation result by OCD and ASR-VE.

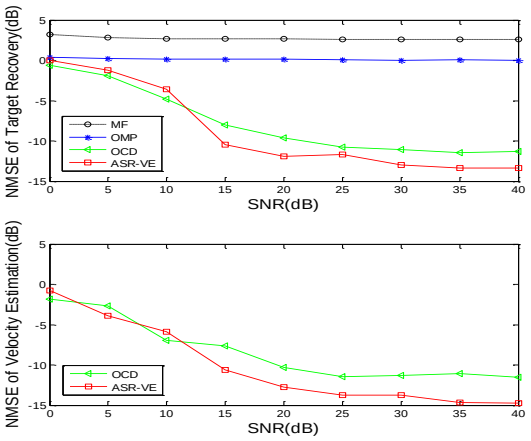

Fig. 5. NMSE of target recovery and velocity estimation (only for OCD, ASR-VE) results versus SNR by MF, OMP, OCD, ASR-VE

V. Conclusions

In this paper, we propose a new approach of adaptive sparse recovery via velocity estimation (ASR-VE) for multiple moving targets FD-MIMO radar imaging. ASR-VE can adaptively estimate the velocities of the targets and then alleviate the mismatch of the sensing matrix, at last, obtain good recovery performance and velocity estimation. Besides, benefited from adaptively velocity and norm p adjusting and updating, ASR-VE has some merits, e.g., better recovery performance, improved robustness to noise, accelerated converge to the true value. The derivations and numerical simulations illustrate the effectiveness of the new method, which shows the potential for the method to be applied in practical systems.

References

[1] E. Fishler, A. Haimovich, R. Blum, D. Chizhik, L. Cimini, and R. Valenzuela, "MIMO radar: An idea whose time has come," *IEEE Radar Conference*, pp.71-78, 2007.

[2] J. J. Zhang and A. P. Suppappola, "MIMO radar with frequency diversity," in *Proc. Int. Waveform Diversity Design(WDD) Conference*, pp.208-212, 2009.

[3] C. C. Liu and W. D. Chen, "Sparse frequency diverse MIMO radar imaging," presented at 46th Asilomar Conference on Signals, Systems, and Computers, 2012.

[4] C. Y. Chen and P. P. Vaidyanathan, "Compressive sensing in MIMO radar," *42nd Asilomar Conference on Signals, Systems and Computers*, pp.41-44, 2008.

[5] Y. Yu, A. P. Petropulu, and H. V. Poor, "CSSF MIMO radar: Low-complexity compressive sensing based MIMO radar that uses step frequency," *IEEE Trans. Aerospace and Electronic Systems*, vol. 48, no.2, pp.1490-1504, 2012.

[6] L. Wang, M. Cheney, and B. Borden, "Multistatic radar imaging of moving targets," *IEEE Radar Conference*, pp. 391-396, 2010.

[7] A. Hassanien, S. A. Vorobyov, and A. B. Gershman, " Moving target parameters estimation in non-coherent MIMO radar systems," *Arxiv Preprint*, 2012.

[8] Y. Chi, L. Scharf, A. Pezeshki, and A. Calderbank, "Sensitivity to basis mismatch in compressed sensing," *IEEE Trans. Signal Processing*, vol.59, no.8, pp.2182-2195, 2011.

[9] S. Ivana and C. K. William, "Imaging of moving targets with multi-static SAR using an overcomplete dictionary," *IEEE Journal of Selected Topics in Signal Processing*, vol. 1, no. 1, pp. 164-175, 2010.

[10] M. H. Md and M. Kaushik, "Range-Doppler imaging via sparse representation," *IEEE Radar Conference*, pp.486-491, 2011.

[11] Z. Yang, C. Zhang, and L. Xie, "Robustly stable signal recovery in compressed sensing with structured matrix perturbation," *Arxiv preprint*, 2011.

[12] X. Tan, W. Roberts, J. Li, and P. Stoica, "Range-Doppler imaging via a train of probing pulses," *IEEE Trans. Sginal Processing*, vol. 57, no. 3, pp.1084-1097, 2009.

[13] W. G. Carrara, R. S. Goodman, and R. M. Majewski, *Spotlight synthetic aperture radar-signal processing algorithm, Norwood, MA: Artech House*, 1995.

[14] C. V. Jakowatz, D. E. Wahl, and P. H. Eichel, "Refocus of constant-velocity moving targets in synthetic aperture radar imagery," *Algorithms for Synth. Aperture Radar Imagery*, vol. 3370, no. 1, pp. 85-95, 1998.

[15] I. F. Gorodnitsky and B. D. Rao, "Sparse signal reconstructions from limited data using FOCUSS: A re-weighted minimum norm algorithm *IEEE Trans. Signal Processing*, vol. 45, pp. 600-616, 1997.

[16] J. N. Franklin, *Matrix theory*, Dover Pubns, 2000.

[17] C. C. Liu, H. Xu, X. Z. He, and W. D. Chen, "The distributed passive radar 3-D imaging and analysis in wavenumber domain," *IEEE International Conference on Signal Processing (ICSP2010)*, pp. 2051–2054, 2010.

He Xuezhi received the B.E. degree in electrical engineering from University of Science and Technology of China (USTC), Hefei, China, in 2008. He is currently working toward the Ph.D degree in the Department of Electrical Engineering, USTC. His research interests include microwave imaging, array signal processing, and compressive sensing.

Liu Bo received the B.E. degree in electrical engineering from University of Science and Technology of China (USTC), Hefei, China, in 2011. He is currently working toward the M.E. degree in the Department of Electrical Engineering, USTC. His research interests include microwave imaging, array signal processing, and compressive sensing.

Wang Dongjin received the B.Sc. degree in 1982 from University of Science and Technology of China (USTC), Hefei, China, and the M.Sc. degree in 1985 from Nanjing electronic engineering research center. He served as Professor of the Department of Electrical Engineering, USTC. He was previously Dean of the Department of Electrical Engineering, Deputy Dean of the School of Information and Science Technology, USTC, Vice-President of USTC. His interests are in the areas of electromagnetic field and microwave, millimeter-wave technology theory, with applications to digital communications and radar.